In situ study at high pressure and temperature of the environment of water in hydrous Na and Ca alumino-silicate melts…

Article *in* Journal of Geophysical Research: Solid Earth · June 2017

DOI: 10.1002/2017JB014262

CITATIONS
0

READS
44

3 authors, including:

Charles Le Losq
Australian National University
37 PUBLICATIONS **178** CITATIONS
SEE PROFILE

Celia Dalou
Centre de Recherches Pétrographiques et Géoc…
28 PUBLICATIONS **146** CITATIONS
SEE PROFILE

AGU PUBLICATIONS

JGR

Journal of Geophysical Research: Solid Earth

RESEARCH ARTICLE
10.1002/2017JB014262

Key Points:
- Strong hydrogen bonds can form in glasses below their glass transition temperature depending on the glass composition
- Temperature drives the evolution of the O-H stretching signals in Raman spectra of melts and fluids through different processes
- Temperature and chemistry of the bulk system are predicted to drive the behavior of hydrogen isotopes in water-saturated volcanic systems

Supporting Information:
- Supporting Information S1
- Data Set S1
- Data Set S2
- Data Set S3
- Data Set S4
- Data Set S5
- Data Set S6

Correspondence to:
C. Le Losq,
charles.lelosq@anu.edu.au

Citation:
Le Losq, C., C. Dalou, and B. O. Mysen (2017), In situ study at high pressure and temperature of the environment of water in hydrous Na and Ca aluminosilicate melts and coexisting aqueous fluids, *J. Geophys. Res. Solid Earth*, *122*, doi:10.1002/2017JB014262.

Received 30 MAR 2017
Accepted 14 JUN 2017
Accepted article online 23 JUN 2017

In situ study at high pressure and temperature of the environment of water in hydrous Na and Ca aluminosilicate melts and coexisting aqueous fluids

Charles Le Losq[1,2], Célia Dalou[1,3], and Bjorn O. Mysen[1]

[1]Geophysical Laboratory, Carnegie Institution of Washington, Washington, District of Columbia, USA, [2]Research School of Earth Sciences, The Australian National University, Canberra, ACT, Australia, [3]Now at Department of Earth Sciences, University of Minnesota, Minneapolis, Minnesota, USA

Abstract The bonding and speciation of water dissolved in Na silicate and Na and Ca aluminosilicate melts were inferred from in situ Raman spectroscopy of the samples, in hydrothermal diamond anvil cells, while at crustal temperature and pressure conditions. Raman data were also acquired on Na silicate and Na and Ca aluminosilicate glasses, quenched from hydrous melts equilibrated at high temperature and pressure in a piston cylinder apparatus. In the hydrous melts, temperature strongly influences O-H stretching ν(O-H) signals, reflecting its control on the bonding of protons between different molecular complexes. Pressure and melt composition effects are much smaller and difficult to discriminate with the present data. However, the chemical composition of the melt + fluid system influences the differences between the ν(O-H) signals from the melts and the fluids and, hence, between their hydrogen partition functions. Quenching modifies the O-H stretching signals: strong hydrogen bonds form in the glasses below the glass transition temperature T_g, and this phenomenon depends on glass composition. Therefore, glasses do not necessarily record the O-H stretching signal shape in melts near T_g. The melt hydrogen partition function thus cannot be assessed with certainty using O-H stretching vibration data from glasses. From the present results, the ratio of the hydrogen partition functions of hydrous silicate melts and aqueous fluids mostly depends on temperature and the bulk melt + fluid system chemical composition. This implies that the fractionation of hydrogen isotopes between magmas and aqueous fluids in water-saturated magmatic systems with differences in temperature and bulk chemical composition will be different.

Plain Language Summary Water is the main gas released during volcanic eruptions. At depth, prior to eruption, it is dissolved in magmas (also called silicate melts) as water molecules or hydrogen ions bonded to the silicate molecules that build the molecular backbone of magmas. This greatly affects the silicate melt properties and, in turn, determines the behavior of volcanic eruptions at surface or the mobility of magmas in the Earth crust. In this regard, it is important to know how water reacts with the molecules constituting silicate melts. In this study, we looked at how water dissolves in silicate melts as a function of temperature, pressure, and melt chemical composition. Results show that the molecular environment of water mostly is affected by temperature. The chemical composition of the aqueous fluid-silicate melt bulk system further influence the solubility of the two phases in each other and, hence, the differences between the water environment in the two phases. This, in turn, may affect the partitioning of hydrogen isotopes between magmas and aqueous fluids in the Earth crust and, hence, our use of hydrogen isotopes to study magmatic systems.

1. Introduction

The study of water in silicate melts is of fundamental importance to understand various geologic processes, as water exerts a profound influence on the properties of silicate melts, as for instance, liquidus temperatures [*Kushiro et al*., 1968a, 1968b; *Kushiro*, 1969], density and buoyancy [*Richet and Polian*, 1998; *Ochs and Lange*, 1999; *Richet et al*., 2000; *Malfait et al*., 2014], and viscosity [*Leonteva*, 1940; *Saucier*, 1952; *Shaw*, 1963; *Richet et al*., 1996; *Dingwell et al*., 1996]. However, the environment of protons is still not well known in hydrous melts. Extending the knowledge acquired through Raman, NMR, and IR spectroscopic studies of hydrous glasses [*Scholze*, 1960; *Bartholomew et al*., 1980; *Mysen et al*., 1980; *Stolper*, 1982; *Mysen and Virgo*, 1986; *McMillan and Remmele*, 1986; *Kohn et al*., 1989], in situ studies of molten hydrous silicates confirm that water is present as molecular H_2O (H_2O_{mol}) that reacts with the melt oxygens to form hydroxyl groups [*Nowak and*

Behrens, 1995; *Holtz et al*., 1996; *Sowerby and Keppler*, 1999; *Behrens and Yamashita*, 2008; *Mysen*, 2009, 2010; *Chertkova and Yamashita*, 2015], following the equilibrium:

$$H_2O_{mol\ (melt)} + O^{2-}{}_{(melt)} \Leftrightarrow 2\ OH^-{}_{(melt)}. \quad (1)$$

H_2O_{mol} reacts mostly with bridging oxygens to form T-OH bonds (T = Al, Si), so that water solution in silicate melts results in depolymerization of their structure [*Scholze*, 1960; *Mysen et al*., 1980; *Stolper*, 1982; *Mysen and Virgo*, 1986; *Kohn et al*., 1989; *Zotov and Keppler*, 1998; *Mysen and Cody*, 2005; *Xue and Kanzaki*, 2006; *Mysen*, 2007; *Malfait and Xue*, 2010]. In addition, the formation of M-OH species (with M a metal cation, e.g., Na or Ca) has been documented in silicate and aluminosilicate glasses [*Xue and Kanzaki*, 2004; *Mysen and Cody*, 2005; *Mookherjee et al*., 2008; *Le Losq et al*., 2015b]. Such species may play an important role in determining the effect of water on melt polymerization, because the reaction of water molecules with metal cations does not lead to melt depolymerization [*Xue and Kanzaki*, 2004].

This complex environment of protons in silicate melts results in interesting effects such as, for instance, the intramolecular fractionation of the hydrogen isotopes between different structural positions [*Wang et al*., 2015; *Le Losq et al*., 2016]. This latter effect reflects a complex hydrogen partition function in silicate melts, which influences the fractionation of hydrogen isotopes between silicate melts and minerals or fluids as isotopic partition functions drive partitioning of isotopes between materials [*Bigeleisen and Mayer*, 1947; *Urey*, 1947; *Richet et al*., 1977]. In hydrous silicate melts, the hydrogen partition function is linked to the frequency of the O-H stretching vibrations in H_2O_{mol} and OH^- species (O-H stretching vibrations will be referred as ν(O-H) in the following). Temperature and melt composition influence ν(O-H) vibrations in hydrous silicate melts. For instance, the ionic field strength of metal cations and, to a lesser extent, the Al_2O_3 and SiO_2 concentration influence the ν(O-H) stretching signal shape in hydrous glasses [*Mysen and Virgo*, 1986; *Cody et al*., 2005; *Le Losq et al*., 2015a]. Such observations indicate that those compositional variables influence the environment of protons in hydrous glasses, because ν(O-H) frequency is correlated with both O-O distances around protons and the *X* cation ionic field strength along *X-OH* bonds [*Nakamoto et al*., 1955; *Wall and Hornig*, 1965; *Novak*, 1974; *Mysen and Virgo*, 1986; *Libowitzky*, 1999]. Temperature further influences the O-H stretching vibrations in silicate melts because it drives the speciation of protons between H_2O_{mol} and OH^- species [e.g., *Dingwell and Webb*, 1990; *Nowak and Behrens*, 1995; *Behrens and Yamashita*, 2008]. In addition, at temperatures lower than ~500°C, formation of hydrogen bonds in hydrous silicate melts further can play a role in affecting the ν(O-H) signal frequency [e.g., *Holtz et al*., 1996; *Mysen*, 2012] because the strength of hydrogen bonds can influence O-O distances around protons [*Novak*, 1974; *Libowitzky*, 1999]. Therefore, in situ studies of ν(O-H) stretching signals in hydrous melts may help understanding of how proton environment changes as a function of temperature, pressure, and melt composition and thus allow drawing a better picture of water-silicate interactions.

In this work, experiments in an externally heated diamond anvil cell (HDAC) combined with in situ Raman spectroscopy were performed to probe the environment of protons in melts co-existing with aqueous fluids at pressure and temperature conditions relevant to the Earth's interior. We have chosen to perform experiments using the eutectic quartz-wollastonite-anorthite composition because of its relatively low melting temperature under both anhydrous and hydrous conditions [*Osborn and Muan*, 1960; *Boettcher*, 1970] and of the importance of the $CaO\text{-}Al_2O_3\text{-}SiO_2$ system for geologic systems. To further assess the effects of melt composition, temperature, and pressure on the proton environment at high temperature and high pressure, another HDAC experimental series with a sodium tetrasilicate composition was carried out. The data acquired using the hydrous calcium aluminosilicate and sodium silicate compositions were also combined with existing data for a sodium aluminosilicate composition [*Dalou et al*., 2015a]. Raman data acquired on the hydrous Na tetrasilicate and Na and Ca aluminosilicate melts are then compared with Raman data acquired on the corresponding glasses. This allows an evaluation of the effect of quenching on ν(O-H) Raman signals.

2. Methods

In order to determine how the Raman signals assigned to O-H stretching from water dissolved in melts change with temperature, pressure, and melt composition, three starting compositions were studied. The first composition is a Ca aluminosilicate with the ambient-pressure quartz-wollastonite-anorthite eutectic composition (CA composition, abbreviated as CA-2 and CA-3 in the following sections as two batches of

Table 1. Chemical Composition of Anhydrous Glasses[a]

		SiO_2	Al_2O_3	Na_2O	CaO	NBO/T
CA-2	nom. mol%	64.84	9.06	0.00	26.11	0.41
	nom. wt%	62.00	14.70	0.00	23.30	
	meas. wt%	61.91 (40)	14.68 (11)	ND	23.42 (7)	
CA-3	nom. mol%	64.84	9.06	0.00	26.11	0.41
	nom. wt%	62.00	14.70	0.00	23.30	
	meas. wt%	62.20 (36)	14.70 (10)	ND	23.15 (16)	
NS4	nom. mol%	80.00	0.00	20.00	0.00	0.50
	nom. wt%	79.50	0.00	20.50	0.00	
	meas. wt%	79.04 (47)	0.00 (00)	20.96 (11)	ND	

[a]nom. mol%, nom. wt%, and meas. wt% refer, respectively, to the nominal compositions in mol and wt% and to the measured composition in wt%. ND: not detected. Errors are given at the 1σ confidence interval.

glass were synthetized), the second a sodium silicate ($Na_2Si_4O_9$, denoted NS4), and the third a sodium aluminosilicate (NS3A5 from *Dalou et al*. [2015a]). Data for the NS3A5 composition are from *Dalou et al*. [2015a], in which D/H fractionation experiments were performed in a HDAC. We used their experimental series in which the bulk D/H ratio of the fluid is the lowest (0.04), so that the presence of a minor amount of D should not affect the ν(O-H) signals significantly. This assumption seems very reasonable when considering that, in addition to the very low D content in the experimental series, the ν(O-D) and ν(O-H) signals occur at ~2600 and ~3600 cm^{-1}, respectively, and are well distinct in the hydrous NS3A5 melt (e.g., see spectra in *Dalou et al*. [2015a]).

2.1. Starting Materials

Anhydrous glasses (sodium silicate NS4 and two batches of Ca aluminosilicate, CA-2 and CA-3) were synthesized from reagent-grade Na_2CO_3, $CaCO_3$, Al_2O_3, and SiO_2 powders, previously dehydrated at 300, 500, 1100, and 1100°C, respectively. Starting powders were mixed for 1 h in an agate mortar then melted in a Pt crucible. The materials were heated to 1400°C at a rate of 1°C/min to ensure a slow decarbonation process. The melts were quenched to glass in air. After the initial melting, glasses were crushed for 1 h in an agate mortar and refused at 1400°C. This process was repeated three times in order to ensure homogeneous glass starting materials. Analysis of the chemical composition of these glasses was performed by energy dispersive spectrometry (EDS) on a JEOL field emission scanning electron microprobe equipped with an Oxford silicon drift detector. A 15 kV accelerating voltage and a 1.00 nA current were used. Measurements were performed over 25 × 25 μm areas. The data were calibrated with the following standards: cossyrite for Na, pyrope for O and Si, ENAL20 for Al, and diopside for Ca. Calibration was tested on a set of glass standards available at the Geophysical Laboratory. EDS results are within error of standards analyzed as unknowns. Anhydrous CA-2, CA-3, and NS4 glass compositions are reported in Table 1. Preparation and analysis of the Na aluminosilicate glass NS3A5 followed the same protocol [see *Dalou et al*., 2015a].

2.2. CA Glass Hydration Method

Hydrous NS3A5, CA, and NS4 glasses were synthesized by dissolving water in the melts at high temperature and high pressure with a piston-cylinder apparatus. Powdered glass was loaded into ~8 mm long by 3 mm diameter Pt capsules with double-distilled, deionized H_2O (from ~0.3 to ~1.6 μL depending on the desired H_2O concentration). The final amount of added water was determined by weighing the capsules. Loaded and sealed capsules were placed in 3/4 inch tapered diameter furnace assemblies [*Kushiro*, 1976], and held at the desired pressure and temperature for 120 min (Table 2). Temperature was measured with type *S* thermocouples with no correction for pressure on their *emf*, which may be as much as 10°C [*Mao et al*., 1971]. Pressure was calibrated against the melting point of NaCl and the calcite-aragonite transformation [*Bohlen*, 1984]. Estimated uncertainties are ~10°C and ~0.1 GPa, respectively. Final water contents of the glasses were checked with Raman spectroscopy, using the protocol of *Le Losq et al.* [2012].

2.3. Hydrothermal Diamond Anvil Cell Experiments

In situ experiments were performed in an externally heated diamond anvil cell (HDAC) [*Bassett et al*., 1994, 1996] using 1 mm diamond culets. Chips of anhydrous glasses and ^{13}C diamonds (for pressure

Table 2. Details of the Hydrothermal Diamond Anvil Cell Experiments[a]

NS4				CA-2 Run 1				CA-2 Run 2			
T (°C)	ν ^{13}C (cm^{-1})	P (MPa)	Phases	T (°C)	ν ^{13}C (cm^{-1})	P (MPa)	Phases	T (°C)	ν ^{13}C (cm^{-1})	P (MPa)	Phases
25	1277.84	-	-	25	1279.09	-	-	25	1283.81	-	-
200	1275.64	232	F + M + Q	625^{d}	1263.60	n.p.	F + M + W + G + An + *ui*	250^{d}	1280.96	339	F + PW
250	1275.00	339	F + M + Q	700^{d}	1262.29	n.p.	F + M + W + G + An	500^{d}	1275.02	353	F + PW
300	1274.04	361	F + M + Q	800^{d}	1258.34	n.p.	F + M + W + G + An	725^{d}	1267.67	326	F + PW
350	1273.15	441	F + M + Q	850^{d}	1256.71	n.p.	F + M + W + G + An	850^{d}	1263.19	449	F + M + PW
400	1272.30	569	F + M + Q	900^{d}	1254.97	n.p.	F + M + W + An	880^{u}	1264.03	1217	F + M + W
450	1271.10	600	F + M + Q	950^{u}	1253.51	1210.0	F + M + *ui*	900^{d}	1262.30	890	F + M + PW
500	1269.68	583	F + M					920^{u}	1262.91	1430	F + M + W
800	1260.92	1079	SCF					950^{u}	1261.49	1392	F + M

[a]When possible, the phases were identified using signals in the 400–1300 cm^{-1} portion of the Raman spectra. F: fluid, SCF: supercritical fluid, M: melt, Q: quartz, W: wollastonite, PW: pseudo-wollastonite, G: grossular, An: anorthite, *ui*: unidentified mineral phase. Superscript *u* and *d* indicate the measurements during the ramp up (*u*) or ramp down (*d*) of the temperature during the experiments. See supporting information for details.

measurements; see below) were loaded together with triple-distilled and deionized water into the sample chamber, which consists in a central hole in the metal gasket that is squeezed between the two diamonds. A 125 μm thick iridium gasket was used during the experiment with the NS4 glass, with a 500 μm diameter central sample hole. Different gaskets were used during the experiments with the CA-2 composition. Indeed, the latter is expected to melt at ~750–800°C and ~800–1000 MPa [*Boettcher*, 1970], and iridium softens and deforms at $T > 800$°C. Therefore, experiments with the CA composition employed rhenium gaskets of the same dimensions to promote the stability of the sample chamber, as Re is less deformable at high temperature. An interior platinum ring was added to the rhenium gaskets to prevent formation of ReO_2 through contact with water. A small Pt ball was pressed into the hole of the Re gasket using a hydraulic press, then drilled to an inner diameter of 300–350 μm, creating a hole with very smooth walls. This "double-gasket" setup does not deform at temperatures above 800°C. No ReO_2 formation was observed during the experiments as shown by the absence of ReO_2-related peaks in the 800–950 cm^{-1} portion of the Raman spectra, confirming that the Pt ring successfully isolated the sample from the rhenium gasket. Temperature was controlled to within 1°C with chromel-alumel thermocouples in contact with the surface of the upper and lower diamond anvils. The accuracy of the temperature measurements is better than 1% [*Bassett et al.*, 1996].

Pressure inside the cell is governed by the PVT relationship of the aqueous fluid so that at fixed sample volume, increasing temperature results in increasing pressure. Pressure was estimated using the pressure-/temperature-dependent one-phonon Raman shift of the synthetic ^{13}C diamond, calibrated in the 0.1–1500 MPa and 25–800°C ranges by *Mysen and Yamashita* [2010]. N_e emission lines, recorded alongside the Raman spectra of the ^{13}C diamond, were used as references to determine the exact Raman shift of the ^{13}C diamond peak, resulting in ±0.1 cm^{-1} uncertainty. This Raman shift uncertainty represents pressure precision of ±40 MPa. When accounting for uncertainty in the calibration of the Raman shift, the total pressure uncertainty in the experiments was ±110 MPa. Only the ^{13}C Raman shift data from one of the two CA-2 experimental series in which melt formation was observed allowed pressure estimation (Table 2 and Figure 1) because the pressure-temperature path for the other was outside the calibration established by *Mysen and Yamashita* [2010]. Therefore, pressure is reported only for CA-2 run 2 (Table 2). During this experimental series, pressure first reached ~1400 MPa, but then dropped significantly after the heating step at 950°C (Table 2 and Figure 1). This pressure drop may have resulted from the diamonds indenting their tungsten carbide seats, as suggested by the fact that we observed that the diamonds were loose after the experiments. In any case, this event is reflected by the strong curvature of the pressure-temperature path of CA-2 run 2 (Figure 1) as all data points at $T < 850$°C were acquired while ramping the temperature down from the 950°C step.

2.4. Raman Spectroscopy

Raman spectra were recorded using a JASCO® NRS 3100 spectrometer, equipped with holographic gratings, a single monochromator, and a 1024 × 128 Andor DV401-F1 CCD Peltier-cooled detector operating at −70°C.

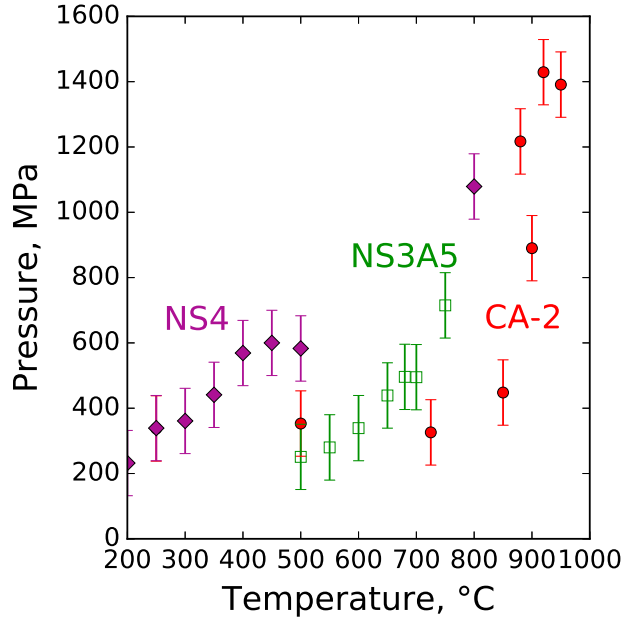

Figure 1. Pressure-temperature paths during the HDAC experiments (see also Table 2).

A 490 nm line of a coherent solid-state laser was used for sample excitation, with a power of ~33 mW on sample. The laser was focused on samples through a 50X Mitutoyo objective lens. During HDAC experiments, Raman spectra of melt, fluid, and crystal phases were recorded using a 1200 grooves/mm grating. Raman spectra of ^{13}C diamonds, recorded with the N_e reference line for pressure estimates, were acquired using a 2400 grooves/mm grating to ensure the best spectral resolution. Alignment of the Raman spectrometer was tested against the 520.7 cm^{-1} Raman peak of pure Si. All spectra reported in this study are unpolarized.

In situ HDAC Raman spectra required a particular processing protocol after acquisition. In the 2700–4000 cm^{-1} range, which comprises the frequency region of second-order Raman signals from the diamonds in the diamond cell itself, backgrounds were subtracted using polynomial baseline functions implemented in the Spectra.jl library [*Le Losq*, 2016]. The baseline-corrected spectra were then normalized to their total area. In the 600–1300 cm^{-1} range (see Figure S1 in the supporting information), the spectra are affected by strong signals from the diamond vibration at ~1332 cm^{-1}. To remove the diamond's effect on the spectra, we followed a protocol similar to that used in *Dalou et al.* [2015a] to remove second-order diamond signals from D-O stretching signals. We acquired a Raman spectrum of the diamond anvil (*diamond spectrum*), pointing the laser on the gasket without changing its optical focus, immediately after acquisition of a sample Raman spectrum (*sample spectrum*). Using the visible diamond signals in the 1220–1270 and 1340–2499 cm^{-1} portions of the Raman spectra where no sample signals are expected, a least squares routine corrects the diamond and sample spectra for any wave number shift, and adjusts the diamond signal in the diamond spectrum to that in the sample spectrum. This allows obtaining diamond-subtracted Raman spectra. Their intensities are then corrected for temperature and excitation line effects using the equation from *Long* [1977] implemented in the Spectra.jl library. Finally, the intensities of the corrected spectra are normalized to the total integrated intensity measured between 600 and 1250 cm^{-1}.

3. Results

3.1. Observations During the HDAC Experiments

Silicate melts in equilibrium with aqueous fluids were observed in the experimental series with the NS4 composition and in two series with the CA-2 composition. Table 2 summarizes the phases observed and the pressure and temperature conditions of the experiments. Additional details about the CA-2 experiments are provided in the supporting information.

During the NS4 experimental series, the temperature was initially increased to 800°C (see pressure-temperature path in Figure 1 and Table 2). At such conditions, a single supercritical fluid was observed (Table 2). During cooling to 500°C, phase separation of a silicate melt and an aqueous fluid was observed at ~530°C. Quartz crystals grew from this composition when cooling to 450°C. Between 500 and 200°C, the cell was cooled in ~50°C steps, and held for 1 h between steps (Table 2). In situ Raman spectroscopy measurements were acquired during those 1 h periods.

The first experimental series with the CA-2 composition was an exploratory run, in which the temperature was first increased up to 900°C at a rate of 1°/s (run 1 in Table 2). During this first heating ramp, the initial

glass fully crystallized. Melt appeared at ~870°C as small blobs between crystals. The melt proportion increased as the temperature was increased to 950°C. The sample was left at this temperature for ~2 h to ensure chemical and thermal equilibrium before any further pressure and temperature change. Additional observations were performed at 900, 850, 800, and 700°C. The sample was held at each temperature for at least 1 h. Complete crystallization of the melt was observed upon cooling to 625°C. Three crystalline phases (wollastonite, grossular, and anorthite) were distinguished with the aid of Raman spectroscopy between 900 and 625°C (see Text S1 and Figure S1 in the supporting information comparing melts and crystal spectra from the RRUFF database [*Lafuente et al*., 2015]). However, because of the small size of melt blobs, no Raman measurement of the O-H stretching signal from the melt phase was possible without contamination by the signal from adjoining fluid. Therefore, no Raman data for the O-H stretching signal in the melt phase are reported for the first experimental series with the CA-2 composition.

During the second experimental series with the CA-2 composition (run 2 in Table 2), the melt phase appeared at ~880°C during heating (880^{up} in Table 2). The melt was in equilibrium with an aqueous phase and wollastonite crystals. As temperature was increased further, crystals disappeared at 940°C, such that only the melt and aqueous fluid phases remained at 950°C. Raman spectra were recorded at 880 and 950°C during heating, and then during cooling at 900, 850, 725, 500, and 250°C. The sample was held at each temperature for at least 1 h during cooling. Widespread crystallization of acicular pseudowollastonite occurred with decreasing temperature from 850 to 725°C. At 500 and 250°C, the Raman shift of the ^{13}C peak was measured to constrain the pressure-temperature path, but the presence of melt could not be assessed due to the extensive amount of pseudowollastonite needles in the sample chamber.

3.2. O-H Raman Signals

In the 3000–4000 cm^{-1} frequency range, asymmetric broad peaks with intensity maxima centered between ~3535 and ~3575 cm^{-1} were observed in the Raman spectra of all melts and fluids (Figure 2). Those signals are assigned to ν(O-H) vibrations in the melts and fluids [*Hibben*, 1933, 1937; *Scholze*, 1960; *Walrafen*, 1975]. The ν(O-H) signals in the Raman spectra of the melts are more asymmetric than those in the Raman spectra of the fluids with which they were in equilibrium (Figure 2). This is particularly visible in the signals acquired during the second CA-2 experimental series. Indeed, for a given composition, the frequency and the half width at half maximum (HWHM) of the ν(O-H) peak are different between the melts and coexisting fluids (Figure 3). In general, the HWHMs of the ν(O-H) peaks in the fluid Raman spectra are lower than those in the melt Raman spectra. The ν(O-H) frequencies in the fluid Raman spectra are also higher than those in the melt Raman spectra in the NS3A5 and CA-2 experimental series, but the inverse relationship is observed for the NS4 experimental series.

The frequencies of the ν(O-H) peaks in the fluid and melt Raman spectra increase with increasing temperature (Figure 3a). The rate of this increase is not the same between the different experimental series. Indeed, while increasing temperature between 200 and 450°C results in large ν(O-H) frequency changes in the NS4 experimental series, increasing temperature between 500 and 700°C results in a much more moderate increase of the ν(O-H) frequency in the NS3A5 experimental series. A systematic trend is even more difficult to draw for the CA-2 experimental series. If we consider the melt point at 850°C as an outlier (this melt spectrum probably is affected by some fluid signal, as its ν(O-H) frequency and HWHM suggest; see Figure 3), a decrease of the ν(O-H) frequency in the melt Raman spectra is barely detectable. Some scatter of the points is also observed for the fluid Raman spectra.

Observation of the ν(O-H) peak HWHM corroborates the general effect of temperature on melt and fluid ν(O-H) signals (Figure 3b). A large, general decrease of the ν(O-H) peak HWHMs is observed at low temperature in the NS4 experimental series. The ν(O-H) peak HWHMs in spectra of fluids and melts are affected at the same rate. In the NS3A5 experimental series at $T > 500$°C, the fluid ν(O-H) peak HWHM changes much less than that of the melt. Finally, the fluid and melt ν(O-H) peak HWHMs in the CA-2 experimental series are nearly constant, considering again the melt point at 850°C as an outlier. We finally note that, in general, the differences between the fluid and melt ν(O-H) peak HWHMs and frequency are higher for the CA-2 experimental series than for the NS3A5 and NS4 experimental series.

The Raman shift centroids of the ν(O-H) fluid and melt signals can be calculated by integrating the Raman shifts as a function of their associated intensities. Variations of the centroids take into account both the

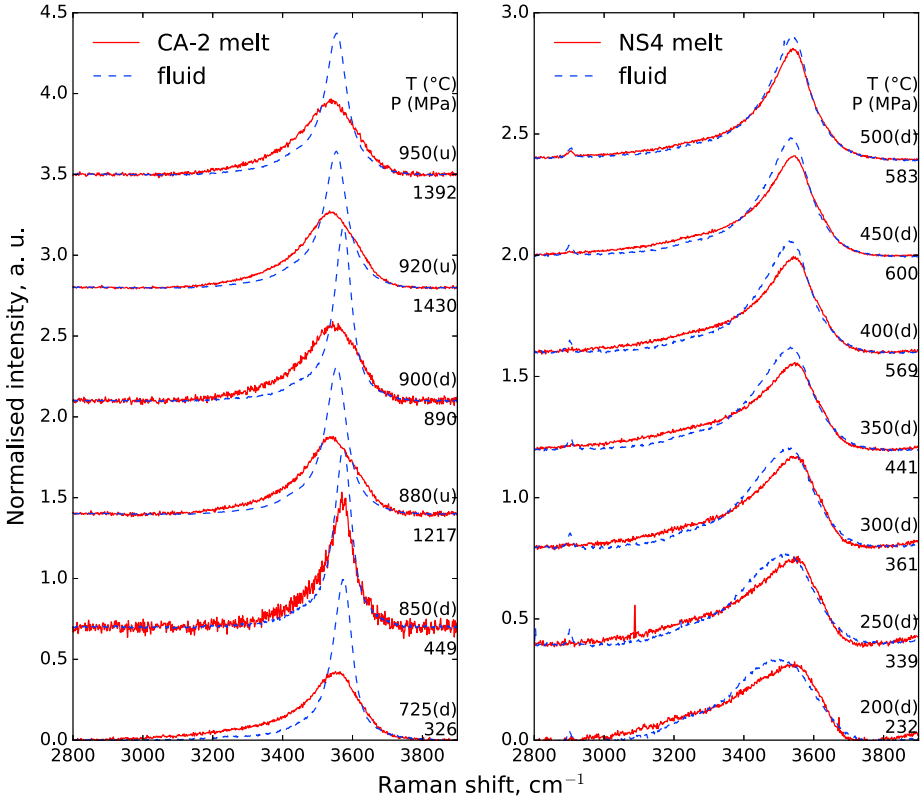

Figure 2. The 2800–3900 cm^{-1} portion of Raman spectra showing signals assigned to O-H stretching in the melts and fluids during successful experimental series with NS4 and CA-2 (run 2) compositions. The letters *u* and *d* in the parentheses after the temperatures indicate the measurements during the ramp up (*u*) or the ramp down (*d*) of the temperature during the experiments (see also Table 2). The small peak around 2910 cm^{-1} in the Raman spectra of the fluid in the NS4 experimental series is assigned to C-H stretching, its presence reflecting a low level of carbon impurities in the fluid during this experimental series. Processed spectra are provided in the supporting information.

changes in frequency and HWHM of the peaks driven by changes in composition and temperature. The centroids of the ν(O-H) Raman signals from fluids are systematically higher than those of the ν(O-H) signals from melts (Figure 4). The centroids generally increase with increasing temperature for both melts and fluids (Figure 4), but at different rates. In the fluids, the ν(O-H) signal centroid increases of ~20 cm^{-1} below 350°C in

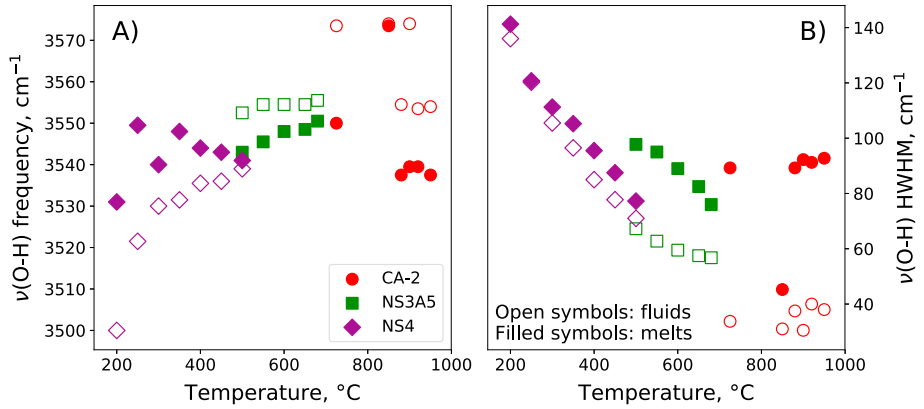

Figure 3. (a) Frequency at the intensity maximum and (b) half width at half maximum (HWHM) of the band assigned to O-H stretching in the different melts (filled symbols) and coexisting fluids (open symbols) as a function of temperature. The outlier melt CA-2 point at 850°C is probably due to noise in the Raman spectrum at this particular temperature (see Figure 2).

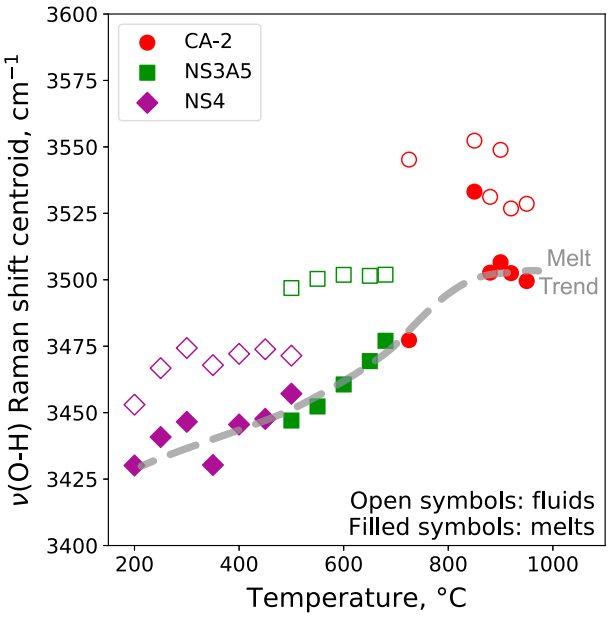

Figure 4. Frequency centroid of the band assigned to O-H stretching in the different melts (filled symbols) and coexisting fluids (open symbols) as a function of temperature. The plateau formed by data from the CA composition suggests that the O-H stretching signal did not change above 800°C. The outlier melt CA-2 point at 850°C is probably due to noise in the Raman spectrum at this particular temperature (Figure 2).

the NS4 experimental series, then level off at a value of ~3472 cm^{-1}. In the NS3A5 experimental series, the centroids in the fluid Raman spectra are nearly constant at a value of ~3500 cm^{-1}, and in the CA-2 experimental series scatter around a value of 3538 cm^{-1}. In the latter case, such scatter probably originates from the scatter of the ν(O-H) Raman shift in the CA-2 fluid Raman spectra (Figure 3a) and may be explained by the large changes in pressure that occurred in the second CA-2 experimental series (Figure 1). This effect seems to affect the fluid more than the melt. In all cases, the ν(O-H) centroids in the melt Raman spectra are more affected by the temperature increase than those in the fluid Raman spectra. Indeed, the ν(O-H) centroids in the NS4, NS3A5, and CA-2 melt Raman spectra describe a general increasing trend with increasing temperature (gray dashed line in Figure 4), which is not significantly affected by changes in melt composition and pressure between the different experimental series. Then, for temperatures ranging from 880 to 950°C, ν(O-H) centroids in the CA-2 melt Raman spectra are constant at a value of 3502 ± 3 cm^{-1}.

4. Discussion

4.1. Effects of Temperature on the Proton Environment in Hydrous Silicate Melts

Spectral changes as the system temperature changes observed in Figures 3 and 4 reflect changes in the bonding that involve protons as well as in the O-O distances around protons. Indeed, the O-H stretching frequency is influenced by several factors. At ambient temperature in hydrous crystals, O-O distances and hydrogen bond strength in O-H···O bonds (with ··· a hydrogen bond) as well as O-H stretching frequencies are correlated [*Nakamoto et al.*, 1955; *Wall and Hornig*, 1965; *Novak*, 1974; *Libowitzky*, 1999]. Data on glasses and minerals further show that the ionic field strength of the X cation along X-O-H bonds influence the O-H bond length and, hence, ν(O-H) stretching frequency [*Mysen and Virgo*, 1986; *Beckenkamp and Lutz*, 1992; *Libowitzky*, 1999]. Therefore, the variations in ν(O-H) signals in the Raman spectra of the melts and fluids originate from differences in hydrogen bonds extent and X-OH bonding. The former effect will be important only at temperatures below ~450°C because the formation of hydrogen bonds becomes ineffective at higher temperatures [*Walrafen et al.*, 1986; *Frantz et al.*, 1993; *Holtz et al.*, 1996; *Mysen*, 2012].

At $T < 450$°C, the large variations of the ν(O-H) signals from the melts and fluids in the NS4 experimental series probably are related to the rupture of hydrogen bonds. An enthalpy of hydrogen bond rupture of 8.5 ± 3.0 kJ mol^{-1} can be calculated from the NS4 melt data, a value in good agreement with the previous reports of ~10–11 kJ mol^{-1} for hydrous melts in the Na_2O-Al_2O_3-SiO_2 system [*Mysen*, 2013; *Dalou et al.*, 2015b]. The absence of additional changes in the ν(O-H) signals from the fluids in the NS4 or NS3A5 experimental series at $T > 400$°C (Figures 2–4) corroborates the fact that the occurrence of hydrogen bonds is not important at temperatures above 400–450°C in silicate-saturated fluids. This probably also is the case in the hydrous silicate melts, a statement corroborated by the data of *Holtz et al.* [1996]. Indeed, the latter have shown that the ratio between the ν(O-H) signals and the silicate signal at ~800 cm^{-1} in hydrous SiO_2 glasses first decrease strongly with increasing T between ~20°C and 400°C, and then level off with

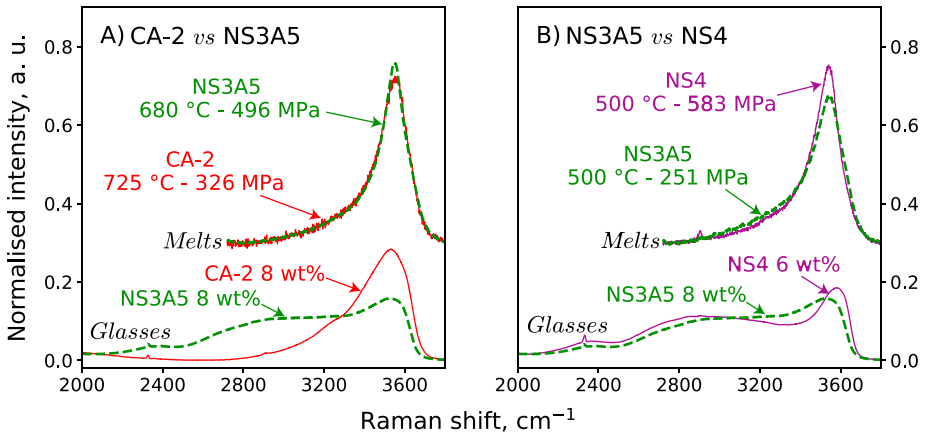

Figure 5. Comparison of O-H stretching signals (a) between CA-2 and NS3A5 melts and glasses and (b) between NS3A5 and NS4 melts and glasses. The glass water content is indicated on the right side of the composition name in wt%. Broad peaks at ~2300 and 2800 cm^{-1} in the Raman spectra of the Na-bearing glasses indicate the presence of strong hydrogen bonds at room temperature. The Raman analysis of the hydrous glasses returned water concentration values of 7.54 ± 0.26 wt% H_2O in the CA glass and 8.0 ± 0.2 wt% H_2O in the NS3A5 glass; the NS4 + 6 wt% glass was analyzed in *Le Losq et al.* [2015a].

further increases of *T*. In their experiments, no change of the speciation of the protons was observed, such that observed changes were assigned to rupture of hydrogen bonds. Their experiments thus support the statement that, as observed in fluids, hydrogen bonds exist up to *T*~450°C in silicate glasses and melts, but are not an important bonding mechanism at higher temperatures.

As a result, at $T <$ ~450°C, the evolution of the ν(O-H) signals from the hydrous melts reflect both changes in the hydrogen bond framework and in the covalent bonding of protons between different H_2O_{mol}, T-OH, and M-OH molecular complexes. At $T >$ ~450°C, only the changes in the covalent bonding of protons drives the changes in the proton environment and, hence, in the ν(O-H) signals. In particular, the increasing interconversion of H_2O_{mol} in OH^- groups with increasing temperature [*Dingwell and Webb*, 1990; *Nowak and Behrens*, 1995] probably explains the ν(O-H) centroid evolution in the melt Raman spectra. The relatively constant frequency and HWHM of the ν(O-H) peaks in the melt Raman spectra in the CA-2 experimental series between 880 and 950°C further reflect a high fraction of hydroxyl groups in the melt at such high temperatures. For instance, the model of *Moretti et al.* [2014] predicts that OH^- groups should represent ~70% of water dissolved in the melt at such temperatures.

4.2. The Effects of Melt Composition and Pressure

The general trend between the ν(O-H) signal centroid data from melts and temperature (Figure 4) suggests that melt composition and pressure effects on ν(O-H) signals are small. Temperature seems to be the main parameter driving the evolution of the ν(O-H) signals through its large influence on hydrogen bonds and proton speciation. Such observation is corroborated by the comparison of the ν(O-H) Raman signals from different melts at similar conditions. For instance, the intensities of the O-H Raman signals from the CA-2 and NS3A5 melts differ by less than 1% at comparable pressure-temperature conditions (Figure 5a). Therefore, despite large differences in initial melt chemical composition (Table 1) and, in particular, in the ionic field strength of the metal cation in the melts (Z/r^2 Na^+ = 0.83 versus Z/r^2 Ca^{2+} = 1.71 A^{-2}, assuming CN = 6 with ionic radius *r* from *Whittaker and Muntus* [1970]), the proton environment in the NS3A5 and CA-2 melts does not differ strongly at the high temperatures shown in Figure 5a (725°C and 680°C for CA-2 and NS3A5, respectively). The ν(O-H) signals in the Raman spectra of the NS4 and NS3A5 melts also are comparable: they differ by only ~3%, despite a factor of 2 in pressure difference between those experiments (Figure 5b). A slight asymmetry of the ν(O-H) peak in the NS3A5 melt spectrum is observed (signal intensities are above the NS4 melt spectrum near 3620 and 3200 cm^{-1}), whereas the ν(O-H) peak in the NS4 melt spectrum is more symmetric. This difference may arise from the presence of aluminum in the NS3A5 melt (compared to the Al-free NS4) or from the pressure difference (Figures 1 and 5). The present data do not allow us to discriminate between those factors. In all cases, in situ Raman spectra of the hydrous NS4, NS3A4, and CA-2 melts

indicate that temperature is the first factor controlling the ν(O-H) signals in the spectra of those materials, confirming previous observations of *Mysen* [2009, 2010].

The extent of the differences between the ν(O-H) signals in the Raman spectra of the melts and in those of the fluids depends mostly on the bulk system composition, as shown by the differences in ν(O-H) frequency, HWHM, and centroid between the melt and fluid Raman spectra (Figures 3 and 4). These are larger in the CA-2 experimental series than in the NS4 experimental melt series. Such differences may originate from different solubility of the silicate component in the aqueous fluids. Indeed, the solubility of Na-bearing silicate components is ~3 times higher than that of Ca-bearing silicate components in aqueous fluids [*Mysen*, 2002]. As a result, the fluid and melt composition are less different in the NS4 experimental series than in the CA-2 experimental series, thus explaining why ν(O-H) Raman signals from melts and fluids are more similar in the former compositional system (Figures 2–4).

4.3. Melt Versus Glass: Quench Effect on Hydrogen Bonds

Two peaks at ~2350 and ~2700 cm^{-1} are visible in the Raman spectra of NS4 and NS3A5 glasses with 6 and 8 wt% water, respectively (Figure 5). The ν(O-H) Raman signals below 3000 cm^{-1} are not observed in the Raman spectra of the NS4 and NS3A5 melts (Figures 2 and 5), even at temperatures as low as 200°C in the NS4 experimental series (Figure 2). At that temperature, the NS4 melt actually should probably be considered a glass. Indeed, the quench of the NS4 melt to glass at *T*~300°C may explain the kinks observed in the ν(O-H) centroid versus temperature relationships (Figure 4). Such a glass transition temperature value is consistent with those reported for similar hydrous sodium tetrasilicate compositions [*Behrens and Yamashita*, 2008].

The ν(O-H) Raman signals below 3000 cm^{-1} indicate the presence of strong hydrogen bonds in the structure of the hydrous glasses [*Novak*, 1974; *Uchino et al*., 1991; *Zotov and Keppler*, 1998]. Therefore, the present data show that strong hydrogen bonds (significantly shortened O-H···O bond length) in the Na silicate and aluminosilicate glasses are only observed at $T < 200$°C. Strong hydrogen bonds thus rupture upon the first steps of heating and do not exist at high temperatures in the hydrous melts. As indicated in section 4.1, only weak hydrogen bonds remain in the melts at temperatures up to ~450°C.

4.4. Hydrogen Bonds and Hydrous Glass Chemical Composition

Contrary to the observations in the Raman spectra of the melts, the ν(O-H) signals in the Raman spectra of the NS4, NS3A5, and CA-2 glasses with comparable amounts of water are quite different (Figure 5). In particular, the ν(O-H) signals at Raman shifts between 2300 and 3000 cm^{-1} are significantly more intense in the NS4 and NS3A5 glass Raman spectra than in that of the CA-2 glass. Slight differences in ν(O-H) signal intensity and frequency also are observed between the Raman spectra of the NS4 and NS3A5 glasses with 6 and 8 wt% water, respectively. Overall, the Raman spectra of the Na-bearing glasses present two peaks at ~2350 and ~2700 cm^{-1} that are absent in that of the CA glass (Figure 5). Therefore, in the chemical domain investigated in this study, compositional differences result in small differences in ν(O-H) signal shape in the Raman spectra of melts at comparable conditions but large differences in those of glasses. In particular, the presence and absence of strong hydrogen bonds in the Na- and Ca-bearing glasses, respectively, corroborate previous findings that indicated that decreasing the ionic field strength of the metal cation in hydrous glasses leads to the formation of strong hydrogen bonds [*Mysen and Virgo*, 1986; *Kohn et al*., 1989; *Xue and Kanzaki*, 2004; *Le Losq et al*., 2015a].

5. Implications

The speciation and bonding of protons in hydrous silicate glasses reflect those in the melts at their glass transition temperature T_g [*Dingwell and Webb*, 1990; *Nowak and Behrens*, 1995]. The covalent bonding of protons thus is fixed below T_g in the glassy state. On the other hand, the present data confirm that hydrogen bonds can form below T_g in the glassy state, through an unknown process that depends on the ionic field strength of metal cation in the glass. This affects ν(O-H) signals in glasses, which become inadequate to draw a picture of the hydrogen environment and partition function in the molten state near T_g. This finding further motivates the need for additional in situ data regarding hydrous melts.

The present in situ Raman data confirm that temperature is the main variable driving changes in ν(O-H) stretching signals in hydrous Na silicate and Na and Ca aluminosilicate melts. Melt composition and

pressure effects are weaker than that of temperature. Temperature is thus the main driver of the hydrogen partition function in silicate melts. In addition, the system bulk composition (fluid + melt) affects the difference between the melt and fluid ν(O-H) signals and, hence, between their hydrogen partition functions, because of its effect on the solubility of the fluid and melt components in each other. As a result, the partitioning of hydrogen isotopes between magmas and aqueous fluids in fluid-saturated magmatic systems is predicted to vary as a function of system composition and temperature.

Acknowledgments
We thank Robert Dennen for his very helpful comments and corrections of the present manuscript. The constructive comments and corrections from Iona McIntosh (JAMSTEC) and an anonymous reviewer were very helpful and appreciated. C. Le Losq thanks for the support from the Carnegie Postdoctoral Fellowship and partial support from Australian Research Council grant FL130100066 to Hugh St. C. O'Neill (Research School of Earth Science–The Australian National University) during the data treatment and the preparation of this manuscript. The HDAC/Raman spectroscopic laboratory was supported in part by NSF grant EAR1212754 to Bjorn O. Mysen. Raman data are available in Data Sets S1–S6 in the supporting information.

References

Bartholomew, R. F., B. L. Butler, H. L. Hoover, and C. K. Wu (1980), Infrared spectra of a water-containing glass, *J. Am. Ceram. Soc.*, *63*(9–10), 481–485, doi:10.1111/j.1151-2916.1980.tb10748.x.

Bassett, W. A., A. H. Shen, M. Bucknum, and I. M. Chou (1994), A new diamond cell for hydrothermal studies to 2.5 GPa and from −190°C to 1200°C, *Rev. Sci. Instrum.*, *64*, 2340–2345.

Bassett, W. A., T. C. Wu, I. M. Chou, H. T. Haselton Jr., J. Frantz, B. O. Mysen, W. L. Huang, K. Sharma, and D. Schiferl (1996), The hydrothermal diamond anvil cell (HDAC) and its applications, in *Mineral Spectroscopy*, edited by R. G. Burns, *Geochem. Soc. Spec. Publ.*, 261–272.

Beckenkamp, K., and H. D. Lutz (1992), Lattice vibration spectra part LXXII. OH stretching frequencies of solid hydroxides—Correlation with structural and bonding data, *J. Mol. Struct.*, *270*, 393–405, doi:10.1016/0022-2860(92)85042-F.

Behrens, H., and S. Yamashita (2008), Water speciation in hydrous sodium tetrasilicate and hexasilicate melts: Constraint from high temperature NIR spectroscopy, *Chem. Geol.*, *256*, 306–315.

Bigeleisen, J., and M. G. Mayer (1947), Calculation of equilibrium constants for isotopic exchange reactions, *J. Chem. Phys.*, *15*(5), 261, doi:10.1063/1.1746492.

Boettcher, A. L. (1970), The system CaO-Al_2O_3-SiO_2-H_2O at high pressures and temperatures, *J. Petrol.*, *11*(2), 337–379, doi:10.1093/petrology/11.2.337.

Bohlen, S. R. (1984), Equilibria for precise pressure calibration and a frictionless furnace assembly for the piston-cylinder apparatus, *Neues Jahrb. Mineral. Monatsh.*, *9*, 404–412.

Chertkova, N., and S. Yamashita (2015), In situ spectroscopic study of water speciation in the depolymerized $Na_2Si_2O_5$ melt, *Chem. Geol.*, *409*, 149–156, doi:10.1016/j.chemgeo.2015.05.012.

Cody, G. D., B. O. Mysen, and S. K. Lee (2005), Structure vs. composition: A solid-state ^{29}Si NMR study of quenched glasses along the Na_2O-SiO_2-H_2O join, *Geochim. Cosmochim. Acta*, *69*(9), 2373–2384.

Dalou, C., C. Le Losq, and B. O. Mysen (2015a), In situ study of the fractionation of hydrogen isotopes between aluminosilicate melts and coexisting aqueous fluids at high pressure and high temperature—Implications for the δD in magmatic processes, *Earth Planet. Sci. Lett.*, *426*, 158–166, doi:10.1016/j.epsl.2015.06.032.

Dalou, C., B. O. Mysen, and D. Foustoukos (2015b), In-situ measurements of fluorine and chlorine speciation and partitioning between melts and aqueous fluids in the Na_2O-Al_2O_3-SiO_2-H_2O system, *Am. Mineral.*, *100*(1), 47–58, doi:10.2138/am-2015-4859.

Dingwell, D. B., and S. L. Webb (1990), Relaxation in silicate melts, *Eur. J. Mineral.*, *2*, 427–449.

Dingwell, D. B., C. Romano, and K.-U. Hess (1996), The effect of water on the viscosity of a haplogranitic melt under *P-T-X* conditions relevant to silicic volcanism, *Contrib. Mineral. Petrol.*, *124*(1), 19–28, doi:10.1007/s004100050170.

Frantz, J. D., J. Dubessy, and B. Mysen (1993), An optical cell for Raman spectroscopic studies of supercritical fluids and its application to the study of water to 500°C and 2000 bar, *Chem. Geol.*, *106*(1), 9–26, doi:10.1016/0009-2541(93)90163-D.

Hibben, J. H. (1933), Raman spectra in inorganic chemistry, *Chem. Rev.*, *13*(3), 345–478, doi:10.1021/cr60046a001.

Hibben, J. H. (1937), The Raman spectra of water, aqueous solutions and ice, *J. Chem. Phys.*, *5*(3), 166–172, doi:10.1063/1.1750001.

Holtz, F., J. M. Bény, B. O. Mysen, and M. Pichavant (1996), High-temperature Raman spectroscopy of silicate and aluminosilicate hydrous glasses: Implications for water speciation, *Chem. Geol.*, *128*, 25–39.

Kohn, S. C., R. Dupree, and M. E. Smith (1989), Proton environments and hydrogen-bonding in hydrous silicate glasses from proton NMR, *Nature*, *337*, 539–541.

Kushiro, I. (1969), The system forsterite-diopside-silica with and without water at high pressures, *Am. J. Sci.*, *267*, 269–294.

Kushiro, I. (1976), A new furnace assembly with a small temperature gradient in solid-media, high-pressure apparatus, *Carnegie I. Wash. b.*, *75*, 832–833.

Kushiro, I., H. S. Yoder, and M. Nishikawa (1968a), Effect of water on the melting of enstatite, *Geol. Soc. Am. Bull.*, *79*(12), 1685–1692, doi:10.1130/0016-7606(1968)79[1685:EOWOTM]2.0.CO;2.

Kushiro, I., Y. Syono, and S. Akimoto (1968b), Melting of a peridotite nodule at high pressures and high water pressures, *J. Geophys. Res.*, *73*(18), 6023–6029, doi:10.1029/JB073i018p06023.

Lafuente, B., R. T. Downs, H. Yang, and N. Stone (2015), The power of databases: The RRUFF project, in *Highlights in Mineralogical Crystallography*, pp. 1–30, W. De Gruyter, Germany.

Le Losq, C. (2016), Spectra.jl: A Julia package for processing spectroscopic data, doi:10.5281/zenodo.53940.

Le Losq, C., D. R. Neuville, R. Moretti, and J. Roux (2012), Determination of water content in silicate glasses using Raman spectrometry: Implications for the study of explosive volcanism, *Am. Mineral.*, *97*(5–6), 779–790, doi:10.2138/am.2012.3831.

Le Losq, C., G. D. Cody, and B. O. Mysen (2015a), Alkali influence on the water speciation and the environment of protons in silicate glasses revealed by ^{1}H MAS NMR spectroscopy, *Am. Mineral.*, *100*(2–3), 466–473, doi:10.2138/am-2015-5004.

Le Losq, C., B. O. Mysen, and G. D. Cody (2015b), Water and magmas: Insights about the water solution mechanisms in alkali silicate melts from infrared, Raman, and ^{29}Si solid-state NMR spectroscopies, *Prog. Earth Planet. Sci.*, *2*(1), 22, doi:10.1186/s40645-015-0052-7.

Le Losq, C., B. O. Mysen, and G. D. Cody (2016), Intramolecular fractionation of hydrogen isotopes in silicate quenched melts, *Geochem. Perspect. Lett.*, 87–94, doi:10.7185/geochemlet.1609.

Leonteva, A. (1940), Measurements of the viscosity of obsidian and of hydrated glasses, *Izv. Akad. Nauk SSSR Ser. Geol.*, *2*, 44–54.

Libowitzky, E. (1999), Correlation of O-H stretching frequencies and O-H O hydrogen bond lengths in minerals, in *Hydrogen Bond Research*, edited by P. D. P. Schuster and P. D. W. Mikenda, pp. 103–115, Springer, Vienna.

Long, D. A. (1977), *Raman Spectroscopy*, McGraw Hill Higher Education, New York.

Malfait, W. J., and X. Xue (2010), The nature of hydroxyl groups in aluminosilicate glasses: Quantifying Si-OH and Al-OH abundances along the $SiO^{27}Al$-^{29}Si-^{1} NMR spectroscopy, *Geochim. Cosmochim. Acta*, *74*(2), 719–737.

Malfait, W. J., R. Seifert, S. Petitgirard, J.-P. Perrillat, M. Mezouar, T. Ota, E. Nakamura, P. Lerch, and C. Sanchez-Valle (2014), Supervolcano eruptions driven by melt buoyancy in large silicic magma chambers, *Nat. Geosci.*, *7*(2), 122–125, doi:10.1038/ngeo2042.

Mao, H. K., P. M. Bell, and J. L. England (1971), Tensional errors and drift of the thermocouple electromotive force in the single stage, piston-cylinder apparatus, *Carnegie I. Wash.*, *70*, 281–287.

McMillan, P., and R. L. J. Remmele (1986), Hydroxyl sites in SiO_2 glass: A note on infrared and Raman spectra, *Am. Mineral.*, *71*, 772–778.

Mookherjee, M., L. Stixrude, and B. Karki (2008), Hydrous silicate melt at high pressure, *Nature*, *452*(7190), 983–986, doi:10.1038/nature06918.

Moretti, R., C. Le Losq, and D. R. Neuville (2014), The amphoteric behavior of water in silicate melts from the point of view of their ionic-polymeric constitution, *Chem. Geol.*, *367*, 23–33, doi:10.1016/j.chemgeo.2013.12.012.

Mysen, B. O. (2002), Solubility behavior of alkaline Earth and alkali aluminosilicate components in aqueous fluids in the Earth's upper mantle, *Geochim. Cosmochim. Acta*, *66*(13), 2421–2438.

Mysen, B. O. (2007), The solution behavior of H_2O in peralkaline aluminosilicate melts at high pressure with implications for properties of hydrous melts, *Geochim. Cosmochim. Acta*, *71*(7), 1820–1834, doi:10.1016/j.gca.2007.01.007.

Mysen, B. O. (2009), Solution mechanisms of silicate in aqueous fluid and H_2O in coexisting silicate melts determined in-situ at high pressure and high temperature, *Geochim. Cosmochim. Acta*, *73*(19), 5748–5763, doi:10.1016/j.gca.2009.06.023.

Mysen, B. (2010), Structure of H_2O-saturated peralkaline aluminosilicate melt and coexisting aluminosilicate-saturated aqueous fluid determined in-situ to 800°C and ~800 MPa, *Geochim. Cosmochim. Acta*, *74*(14), 4123–4139, doi:10.1016/j.gca.2010.04.024.

Mysen, B. O. (2012), Silicate-COH melt and fluid structure, their physicochemical properties, and partitioning of nominally refractory oxides between melts and fluids, *Lithos*, *148*, 228–246, doi:10.1016/j.lithos.2012.06.005.

Mysen, B. O. (2013), Structure–property relationships of COHN-saturated silicate melt coexisting with COHN fluid: A review of in-situ, high-temperature, high-pressure experiments, *Chem. Geol.*, *346*, 113–124, doi:10.1016/j.chemgeo.2012.10.006.

Mysen, B. O., and G. D. Cody (2005), Solution mechanisms of H_2O in depolymerized peralkaline melts, *Geochim. Cosmochim. Acta*, *69*(23), 5557–5566, doi:10.1016/j.gca.2005.07.020.

Mysen, B. O., and D. Virgo (1986), Volatiles in silicate melts at high pressure and temperature 1. Interaction between OH groups and Si^{4+}, Al^{3+}, Ca^{2+}, Na^{+} and H^{+}, *Chem. Geol.*, *57*, 303–331.

Mysen, B. O., and S. Yamashita (2010), Speciation of reduced C–O–H volatiles in coexisting fluids and silicate melts determined in-situ to ~1.4 GPa and 800°C, *Geochim. Cosmochim. Acta*, *74*(15), 4577–4588, doi:10.1016/j.gca.2010.05.004.

Mysen, B. O., D. Virgo, W. J. Harrison, and C. M. Scarfe (1980), Solubility mechanisms of H_2O in silicate melts at high pressures and temperatures: A Raman spectroscopic study, *Am. Mineral.*, *65*, 900–914.

Nakamoto, K., M. Margoshes, and R. E. Rundle (1955), Stretching frequencies as a function of distances in hydrogen bonds, *J. Am. Chem. Soc.*, *77*, 6480–6486.

Novak, A. (1974), Hydrogen bonding in solids. Correlation of spectroscopic and crystallographic data, *Struct. Bond.*, *18*, 177–216.

Nowak, M., and H. Behrens (1995), The speciation of water in haplogranitic glasses and melts determined by in situ near-infrared spectroscopy, *Geochim. Cosmochim. Acta*, *59*(16), 3445–3450.

Ochs, F. A., and R. A. Lange (1999), The density of hydrous magmatic liquids, *Science*, *283*(5406), 1314–1317, doi:10.1126/science.283.5406.1314.

Osborn, E. F., and A. Muan (1960), Phase equilibrium diagrams of oxide systems, Plate 1. The System $CaO–Al_2O_3–SiO_2$., American Ceramic Society with the Edward Orton Jr. Ceramic Foundation, Columbus, Ohio.

Richet, P., and A. Polian (1998), Water as a dense icelike component in silicate glasses, *Science*, *281*(5375), 396–398, doi:10.1126/science.281.5375.396.

Richet, P., Y. Bottinga, and M. Javoy (1977), A review of hydrogen, carbon, nitrogen, oxygen, sulphur, and chlorine stable isotope enrichment among gaseous molecules, *Annu. Rev. Earth Planet. Sci.*, *5*, 65–110.

Richet, P., A.-M. Lejeune, F. Holtz, and J. Roux (1996), Water and the viscosity of andesite melts, *Chem. Geol.*, *128*(1), 185–197, doi:10.1016/0009-2541(95)00172-7.

Richet, P., A. Whittington, F. Holtz, H. Behrens, S. Ohlhorst, and M. Wilke (2000), Water and the density of silicate glasses, *Contrib. Mineral. Petrol.*, *138*(4), 337–347.

Saucier, H. (1952), Quelques expériences sur la viscosité à haute température de verres ayant la composition d'un granite. Influence de la vapeur d'eau sous pression, *Bull. Soc. Fr. Minéral. Cristallogr.*, *75*, 1–45.

Scholze, H. (1960), Zur Frage der unterscheidung zwischen H_2O-Molekeln und OH-gruppen in gläsern und mineralen, *Naturwissenschaften*, *47*, 226–227.

Shaw, H. R. (1963), Obsidian-H_2O viscosities at 1000 and 2000 bars in the temperature range 700° to 900°C, *J. Geophys. Res.*, *68*(23), 6337–6343, doi:10.1029/JZ068i023p06337.

Sowerby, J. R., and H. Keppler (1999), Water speciation in rhyolitic melt determined by in-situ infrared spectroscopy, *Am. Mineral.*, *84*(11–12), 1843–1849.

Stolper, A. (1982), Water in silicate glasses: An infrared spectroscopic study, *Contrib. Mineral. Petrol.*, *81*, 1–17.

Uchino, T., T. Sakka, and M. Iwasaki (1991), Interpretation of hydrated states of sodium silicate glasses by infrared and Raman analysis, *J. Am. Ceram. Soc.*, *74*(2), 306–313.

Urey, H. C. (1947), The thermodynamic properties of isotopic substances, *J. Chem. Soc. Resumed*, 562–581.

Wall, T. T., and D. F. Hornig (1965), Raman intensities of HDO and structure in liquid water, *J. Chem. Phys.*, *43*(6), 2079–2087.

Walrafen, G. E. (1975), Raman spectra from Si-OH groups in solid optical fibers, *J. Chem. Phys.*, *62*, 297–298.

Walrafen, G. E., M. R. Fisher, M. S. Hokmabadi, and W.-H. Yang (1986), Temperature dependence of the low- and high-frequency Raman scattering from liquid water, *J. Chem. Phys.*, *85*(12), 6970–6982, doi:10.1063/1.451384.

Wang, Y., S. X. Cody, D. Foustoukos, B. O. Mysen, and G. D. Cody (2015), Very large differences in intramolecular D-H partitioning in hydrated silicate melts synthesized at upper mantle pressures and temperatures, *Am. Mineral.*, *100*(5–6), 1182–1189, doi:10.2138/am-2015-4940.

Whittaker, E. J. W., and R. Muntus (1970), Ionic radii for use in geochemistry, *Geochim. Cosmochim. Acta*, *34*, 945–956.

Xue, X., and M. Kanzaki (2004), Dissolution mechanisms of water in depolymerized silicate melts: Constraints from ^{29}Si NMR spectroscopy and ab initio calculations, *Geochim. Cosmochim. Acta*, *68*(24), 5027–5057.

Xue, X., and M. Kanzaki (2006), Depolymerization effect of water in aluminosilicate glasses: Direct evidence from ^{27}Al heteronuclear correlation NMR, *Am. Mineral.*, *91*(11–12), 1922–1926.

Zotov, N., and H. Keppler (1998), The influence of water on the structure of hydrous sodium tetrasilicate glasses, *Am. Mineral.*, *83*, 823–834.